Delft University of Technology

In-mission synergy of science and navigation ephemeris products—Potential benefits for
JUICE statistical Delta-V expenditure and beyond

Hener, J.; Fayolle, S.; Dirkx, D.

Citation (APA)
Hener, J., Fayolle, S., & Dirkx, D. (2025). In-mission synergy of science and navigation ephemeris products—Potential benefits for JUICE statistical Delta-V expenditure and beyond. *Planetary and Space Science*, *255*, Article 106017. https://doi.org/10.1016/j.pss.2024.106017

Important note
To cite this publication, please use the final published version (if applicable).
Please check the document version above.

In-mission synergy of science and navigation ephemeris products—Potential benefits for JUICE statistical Delta-V expenditure and beyond

J. Hener [*], S. Fayolle, D. Dirkx

Department of Aerospace Engineering, Delft University of Technology, Delft, 2629HS, The Netherlands

A B S T R A C T

In 2031 the JUICE spacecraft will perform a multi-flyby tour of the Jovian system. Next to the radiometric tracking that is performed for navigation operations, the dedicated radio science instrument (3GM) collects high-accuracy radiometric measurements during the flybys.

We investigate the capability of the radio science data to provide improved moon state knowledge during navigational operations. We introduce ephemeris updates from radio science data into our simulated navigation operations and examine the potential savings of statistical ΔV for corrective manoeuvres. A navigation orbit determination (OD) solution was simulated for the multi-flyby tour of JUICE, including the resulting state knowledge evolution of the Galilean moons. The OD was extended by an interface for external moon ephemeris updates, which was used to evaluate the impact of radio science generated external ephemerides on the statistical ΔV budgets for post-flyby cleanup manoeuvres.

The moon state knowledge evolution during navigation operation showed a rapid reduction of the a-priori moon state uncertainty, for which the navigational tracking data coverage of the long, early tour arcs was identified as the driving factor. As a result of the longer tracking arcs, the moon state knowledge from navigation data results improves more quickly during the initial phase of the tour. Since the impact of moon state knowledge on the corrective manoeuvres is largest in this initial phase, the comparative analysis of the statistical ΔV cost shows that the adoption of radio science ephemeris products does not effectuate significant ΔV savings. Instead we showed that in order to achieve substantial ΔV savings improvements of Europa's and Ganymede's ephemerides are required ahead of JUICE's arrival.

While the analysis concludes that data synergies are unlikely to benefit the navigational operations, it highlights other potential synergies between the navigation and radio science data. A comparatively strong signature of Io's dynamics was found in the simulated navigation data along the long early tour arcs, which could be leveraged for the benefit of the new global moon ephemeris solutions after JUICE.

1. Introduction

The upcoming JUICE mission (JUpiter ICy moons Explorer) will perform an exploratory tour of the Jovian system, focusing on the outer three Galilean moons Europa, Ganymede and Callisto Grasset et al. (2013). The tour phase of the mission will include multiple flybys of these moons. The multi-flyby tour of the Galilean moons is followed by the Ganymede orbital phase. Fig. 1 shows the Ganymede orbit phases through 2032 and 2033, starting at a semi-major axis of 8000 km and eccentricities up to 0.6 and ending with a circular orbit at 500 km altitude. Scheduled at a nominal duration of 4 months, the circular orbit phase (GCO-500) constitutes the final phase of the mission.

The radio science experiment will provide radiometric range and Doppler tracking data to determine the spacecraft trajectory, Galilean satellite gravity fields, and other geodetic quantities (Cappuccio et al.,

2020, 2022). The PRIDE experiment provides complementary VLBI data (Gurvits et al., 2023; Fayolle et al., 2024), as well as three-way Doppler data from each of its receiving antennas.

Due to the many flybys, these data also provide valuable input to Galilean satellite ephemerides, along with data from *e.g.* the PRIDE experiment (angular position), the JANUS payload (optical imaging, (Della Corte et al., 2014)) and data from past and future missions such as Galileo, Juno and Europa Clipper. Therefore, JUICE is expected to significantly contribute towards more accurate ephemerides of the Galilean moons (Dirkx et al., 2017; Lari and Milani, 2019; Fayolle et al., 2022, 2023b; Magnanini et al., 2024).

Long-term, high-accuracy ephemerides are created from a combination of Earth- and space-based optical and radiometric data, and

---
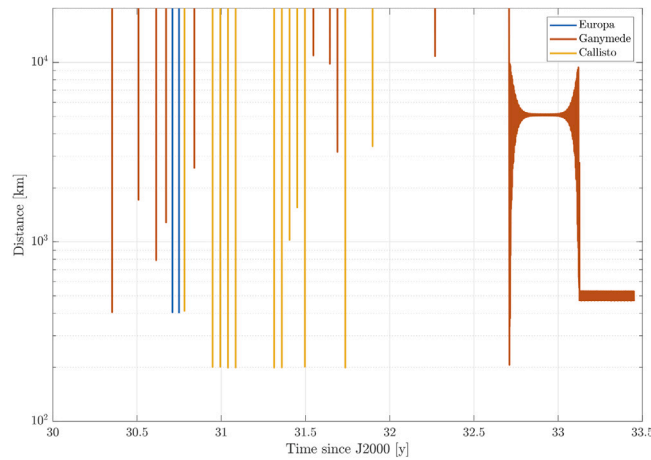
Fig. 1. Distance between the JUICE spacecraft and the Galilean moons during the flyby and orbital phases, based on version 3.2 of CReMA. The vertical lines mark satellite flybys and show the associated closest-approach distances. The first flyby of the tour-phase is taken as flyby "2G2". The earlier 1G1 flyby (Ganymede, h = 400 km), which marks the insertion into the Jovian system (JOI), is omitted.
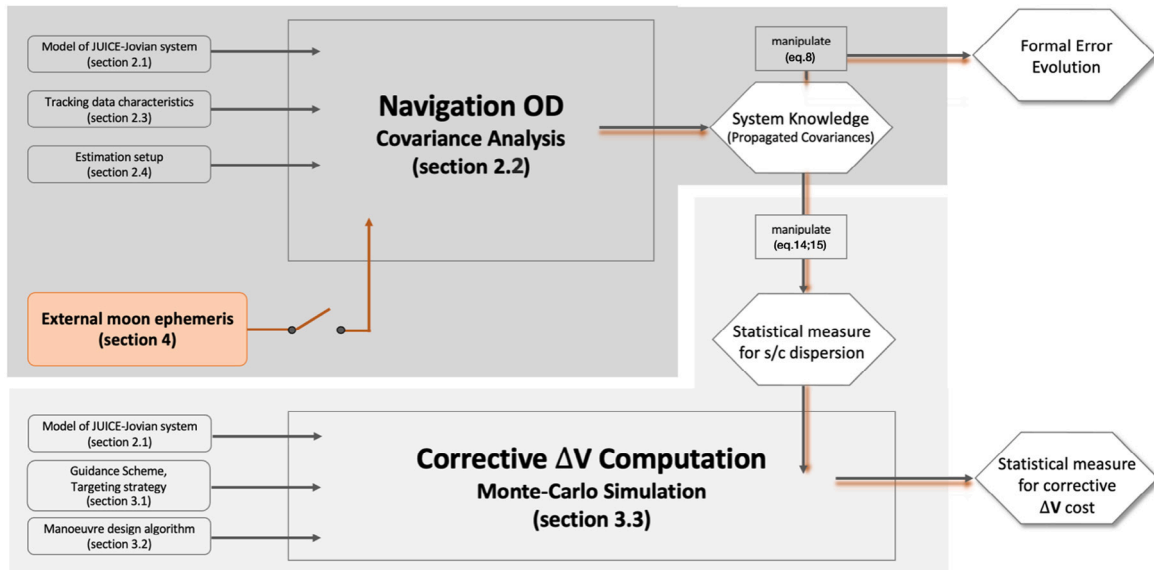
Fig. 2. Schematic overview of the methodological setup of the comparative statistical ΔV analysis. Elements with round edges denote settings and design decisions. Box-like elements represent (an assembly of) implemented functions, that facilitate the computation of relevant results. Results are framed by the hexagonal shapes. The interface for external ephemeris updates is highlighted in orange. The orange trace symbolises the flow of external moon ephemeris knowledge, if introduced via the update interface. When applicable, reference is given to the methodology section, in which the given aspect is presented in more detail.

have important scientific applications: they can help determine tidal dissipation parameters (Lainey and Tobie, 2005; Lainey et al., 2009; Lari et al., 2020) and enable insights into the origin Peale (1999), long-term thermal-orbital evolution (Hussmann and Spohn, 2004; Hay et al., 2020) and the interior processes of natural satellites (Greenberg, 2010; Schubert et al., 2004). High-accuracy ephemerides created using Cassini optical and radio tracking data provided paradigm-shifting insight into the migration rates of the Saturnian moons and the evolution of the system as a whole (Lainey et al., 2020), which has motivated a reconsideration of the mechanisms that drive natural satellite evolution in general (Fuller et al., 2016).

Moon ephemerides also play an important role in the Guidance, Navigation and Control (GNC) operations of the JUICE mission. In the navigation orbit determination (OD), moon state knowledge is periodically updated from dedicated radiometric and optical navigation data (which differ from the science data, see Table 1 (ESOC, 2017–2019; Cappuccio et al., 2020)). Consequently, with each flyby the moon ephemerides are constrained as closely as possible (Ionasescu et al., 2014). Two distinct ephemeris solutions are produced for the

moons: one by the navigation team, and one by the science team. These ephemerides differ significantly, both in the data they use and in their application: navigation solutions prioritise the determination of the short-term spacecraft dynamics with a fast turn-around time (Bellerose et al., 2016; Boone et al., 2017), while science ephemerides prioritise long-term accuracy and tidal parameter determination, without stringent requirements on turn-around time. Moreover, navigation ephemerides are generated and updated throughout the mission, while the science solution is mostly reconstructed after the mission is complete. This explains why there is also a quantitative difference between the two types of moon ephemerides.

In an early study on the Galileo mission (Murrow and Jacobson, 1988), navigation reports of the Cassini mission (Bellerose et al., 2016; Boone et al., 2017) and in the context of Europa Clipper (Ionasescu et al., 2014), the uncertainties of moon ephemerides were identified as an important error source in the navigation OD solutions. Increased moon ephemeris uncertainty increases the uncertainty of the spacecraft

state relative to these moons. This leads to larger target misses during flyby and increased trajectory dispersions and required correction manoeuvres downstream of the flyby (e.g. Martin-Mur et al., 2014).

To mitigate the impact of moon ephemeris uncertainty on flyby targeting performance, Bellerose et al. (2016) report the bi-annual implementation of moon ephemeris updates using external ephemeris products during the Cassini Solstice mission phase. These external ephemerides were generated using more sophisticated setups than the typical navigation solutions.

The practice of external ephemeris updates to the navigation operations could be an attractive option for the JUICE mission to enable a reduction of statistical ΔV expenditure during the flyby tour. Such savings could become important during the consideration of possible mission extensions and enhancements, such as e.g. a lower-altitude orbit after the GCO-500 phase (ESA, 2014).

This work simulates the capabilities of the navigation radiometric data to constrain moon state knowledge and compares it to that of the radio science data. It then assesses the effectiveness of incorporating ephemeris products from the science data into the navigation operations of the JUICE mission, specifically with regards to the ΔV expense of post-flyby correction manoeuvres.

The setup of our analysis is summarised in Fig. 2. First, we simulate the knowledge of the JUICE-Jovian system from navigation data via a covariance analysis (Section 2), both with and without periodic external ephemeris updates based on the science data (as simulated by Fayolle et al. (2022)).

Second, we compute the ΔV expense of corrective manoeuvres (Section 3). Combined with the covariance analysis, this allows us to examine the impact of the aforementioned external ephemeris updates (Section 4) in a comparative statistical ΔV analysis. Using the nominal (*i.e.* update-free) Navigation OD, a baseline for the formal error and the statistical manoeuvre cost is established.

Our comparative application allows for several simplifying assumptions in the setup, so as long as the simplifications affect the baseline and modified cases to a similar extent. The results of our analysis are presented and discussed in Section 5

Simulations in this work rely on the numerical modelling and estimation capabilities of the *Tudat*[1] software (Dirkx et al., 2019), developed at the Astrodynamics & Space Missions department of the Delft University of Technology.

2. Methodology (i) — Orbit determination for navigation

The analysis setup (Fig. 2) includes the simulation of a navigational orbit determination (hereafter "Navigation OD"). The setup was modelled after ESOC (2017–2019), with a number of differences discussed in this section. The results obtained by our Navigation OD implementation, in particular the moons' state covariance evolution, were validated against the covariance data from this reference.

Dynamical modelling of the JUICE spacecraft is discussed in Section 2.1. Section 2.2 describes the concept of covariance analysis, with the characteristics of the simulated observations in Section 2.3. The Navigation OD filter setup and the choice of estimated parameters is presented in Section 2.4.

2.1. Modelling the JUICE-jovian system

The system state vector is denoted by $\mathbf{y}(t)$ as a function of time t. It is propagated numerically from the initial time t_0 along arc i, using

$$\dot{\mathbf{y}} = \mathbf{f}_i(\mathbf{y}, t; \mathbf{p}) \tag{1}$$

where $\mathbf{p}$ denotes parameters of the system dynamics and the state derivative function $\mathbf{f}_i$ is defined by the dynamical model for arc i. State

transition matrices $\mathbf{\Phi}(t, t_0)$ and sensitivity matrix $\mathbf{S}(t)$, which are defined as (Montenbruck and Gill, 2000)

$$\mathbf{\Phi}(t, t_0) = \frac{\partial \mathbf{y}(t)}{\partial \mathbf{y}(t_0)} \tag{2}$$

$$\mathbf{S}(t) = \frac{\partial \mathbf{y}(t)}{\partial \mathbf{p}} \tag{3}$$

are numerically solved concurrently with the state on each arc.

The translational state $\mathbf{x}$ of the JUICE spacecraft (sc) and all Galilean moons (j = 1, 2, 3, 4) are propagated concurrently in a Jovi-centric frame of fixed orientation w.r.t. the International Celestial Reference Frame (ICRF). The system state vector $\mathbf{y}$ thus becomes a vector of size 30:

$$\mathbf{y} = \begin{pmatrix} \mathbf{x}_{sc} \\ \mathbf{x}_1 \\ ... \\ \mathbf{x}_4 \end{pmatrix} \tag{4}$$

Initial states and system parameters for the natural bodies were obtained from the IMCCE ephemerides NOE-5-2021,[2] solar system ephemeris DE432 (Folkner et al., 2014) was used for the position of other solar system bodies. Rotational states of the moons are not propagated, but modelled to be tidally locked with the planet (as is done by *e.g.* Lainey et al., 2004; Dirkx et al., 2016). When propagating the dynamics of the Galilean moons, the following accelerations were taken into account:

- the mutual spherical harmonic acceleration (Lainey et al., 2004; Dirkx et al., 2016) between Jupiter and each Galilean moon j, up to degree and order (D/O) 8/0 for Jupiter, and 2/2 for the moons

- the mutual spherical harmonic accelerations between all Galilean moons, with D/O up to 2/2

Matching the mission profile disseminated in the spice kernels (Acton, 1996) for the JUICE CReMA 3.2 (see Fig. 1),[3] the trajectory of the JUICE spacecraft was simulated for selected arcs of the multi-flyby tour. The selection was limited to arcs including a close flyby ($h < 20000$ km) of a Galilean moon (Fig. 1). This JUICE trajectory was selected to allow for direct comparison and validation with existing navigation analysis by ESOC (2017–2019). It should be noted that the mission profile (CReMA 3.2) that underlies this work has been superseded by profiles from CReMA versions 4 and 5. The results of our analysis were shaped by the main features of the tour profile, namely the long arcs of the early tour stage (2G2, 3G3), the back-to-back placement of the two only Europa flybys as well as the complete absence of Io encounters. Since these features are preserved throughout all CReMA updates, it is expected that the results and conclusions of this work maintain a high degree of relevance for current and future mission profiles.

When propagating the dynamics of the spacecraft during arc i that contains a flyby with moon j, the following accelerations were taken into account:

- the gravitational acceleration of Jupiter's gravity field, up to D/O of 2/0
- the gravitational acceleration of the encountered moon j, considering a gravity field up to D/O 2/2
- the point-mass acceleration of all other Galilean moons.
- acceleration by non-conservative solar radiation pressure, implemented via cannonball model.
- empirical acceleration, absorbing unmodelled dynamical effects — constant (in TNW frame) on 10 day sub-arcs

---

[1] Documentation: https://docs.tudat.space.

[2] https://ftp.imcce.fr/pub/ephem/satel/NOE/JUPITER/
[3] https://www.cosmos.esa.int/web/spice/spice-for-juice

The choice of acceleration models was driven by the requirements of a simulation study, similar to Dirkx et al. (2016), Fayolle et al. (2022), which are less stringent than those of real data analysis. The numerical integration was performed using a Runge–Kutta–Fehlberg method (RKF78), which allows for variable step-size control at an absolute and relative (step-wise) tolerance of 10^{-10} m and a maximum step size of 1000 s. Dynamical model and numerical integration were chosen to ensure consistency between nominal and simulated flyby geometry and timing on each arc.

2.2. Covariance analysis

Given a dynamical model and a set of observations, a covariance analysis maps the formal uncertainty distribution in these observations to formal uncertainty distribution in a set of estimated parameters. Here, we simulate observations of the JUICE mission, and produce estimates using a Navigational OD setup (Section 2.4).

A covariance analysis is valid under a number of assumptions. Firstly, the dynamical model is taken as a perfect description of the system dynamics. Secondly, it is assumed that any sort of systematic measurement errors are accounted for in the observational model, and that the quality of the resulting observations is characterised as uncorrelated Gaussian noise, for which the amplitude is perfectly represented in the weights.

We denote by $\mathbf{h}(T)$ the set of all observations up to time T. A design matrix $\mathbf{H}(T)$ can then be computed for the estimated parameters $\mathbf{q}$ (Montenbruck and Gill, 2000):

$$\mathbf{H}(T) = \frac{\partial \mathbf{h}(T)}{\partial \mathbf{q}} \tag{5}$$

$$\mathbf{q} = [\mathbf{y}_0 ; \mathbf{p} ; \mathbf{s}] \tag{6}$$

where $\mathbf{y}_0$ denotes the initial system state (Eq. (4)), $\mathbf{p}$ and $\mathbf{s}$ are vectors containing parameters of the dynamical and observational models, respectively. The covariance matrix of the estimate of $\mathbf{q}$, considering simulated observations up to time T, is denoted $\mathbf{P_{qq}}(T)$ and is computed as[4]

$$\mathbf{P_{qq}}(T) = \left(\mathbf{P}_{\mathbf{qq},0}^{-1} + \left(\mathbf{H}^T(T)\mathbf{W}(T)\mathbf{H}(T) \right) \right)^{-1} \tag{7}$$

where $\mathbf{P}_{\mathbf{qq},0}$ denotes the *a priori* covariance matrix of the parameter set $\mathbf{q}$ and the weight matrix $\mathbf{W}(T)$, with $W_{ii} = \sigma_{h,i}^{-2}$, accounts for the expected quality of each individual observation.

Taking the square-root of the diagonal entries covariance matrix $\mathbf{P_{qq}}$, one obtains the so-called formal error, which is the expected standard deviation on the estimate of each parameter i:

$$\sigma_i = \sqrt{P_{i,i}} \tag{8}$$

which will typically be an underestimation of the true error, due to the idealising assumptions of a covariance analysis, as discussed in more detail by Dirkx et al. (2017) for the context of the present application.

To mitigate the effect of unmodelled and unestimated errors, we introduce so-called consider parameters. These are not themselves estimated but their uncertainty is considered in the computation of the parameter covariance. The uncertainties associated with the consider parameters are mapped onto the post-fit covariance matrix $\mathbf{P_{qq}}$ as follows (Montenbruck and Gill, 2000)

$$\mathbf{P}_{c,\mathbf{qq}} = \mathbf{P_{qq}} + \left(\mathbf{P_{qq}}\mathbf{H}^T\mathbf{W} \right) \left(\mathbf{H}_c \mathbf{C}\mathbf{H}_c^T \right) \left(\mathbf{P_{qq}}\mathbf{H}^T\mathbf{W} \right)^T \tag{9}$$

where $\mathbf{C}$ denotes the covariance of the consider parameters and $\mathbf{H_c}$ is the associated design matrix (analogous to Eq. (7)).

Using the state transition and sensitivity matrices from Eqs. (2) and (3), the evolving state components of covariance matrices can be propagated from a reference epoch t_0 to any other epoch t:

$$\mathbf{P}_{\mathbf{yy}}^{(t_0 \rightarrow t)}(t) = \left[\boldsymbol{\Phi}\left(t, t_0\right); \mathbf{S}\left(t, t_0\right) \right] \mathbf{P}_{\mathbf{qq}}^{t_0} \left[\boldsymbol{\Phi}\left(t, t_0\right); \mathbf{S}\left(t, t_0\right) \right]^T \tag{10}$$

where $\mathbf{P_{yy}}$ denotes covariance of the system state vector $\mathbf{y}$.

2.3. Tracking data

The Navigation OD of the JUICE spacecraft relies largely on radiometric two-way range and range-rate (Doppler) measurements from Earth-based tracking stations, supplemented by optical navigation data.

Adopting the radiometric data characteristics from ESOC (2017–2019) Doppler data was modelled with 80 µ m/s white noise at an integration time of 1 h, while range observables were taken at a noise level of 10 m at the same cadence (see also Table 1). Additionally, a systematic range observation bias of 2 m was implemented as consider parameter. Occultation and elevation angle ϵ (< 10 degrees) were implemented w.r.t. to the ground station in Malargüe. For this station, a systemic position bias of 30 cm/axis was modelled as a consider parameter (see Section 2.4).

The JUICE Navigation OD combines the radiometric data types with optical navigation (OpNav) images from the navigation camera (Nav-Cam). This data type provides additional information of the relative state of spacecraft w.r.t. observed body. It is used primarily to measure and constrain flyby moon position prior to close encounters, but can also balance the data set by direct observations of Io and Europa. The detailed planning of OpNavs requires a complicated trade-off of observation priorities, geometry and operational constraints and results in a dedicated OpNavs schedule. While OpNavs are included in the filter setup of ESOC (2017–2019), they were omitted from the setup of this study. It is discussed in Section 5.1 that despite this shortcoming our results correspond very well to the estimated moon ephemeris uncertainties from the complete filter of ESOC (2017–2019).

2.4. Estimation setup

We use an arc-wise batch least-squares algorithm, where the covariance is solved on an arc-by-arc basis. A parameter covariance P_{qq} is generated w.r.t. the initial epoch t_0 of every arc i. For this calculation, the filter fuses a batch of measurement data from the given arc i with *a priori* parameter information.

The estimatable parameters are modelled after the reference filter of ESOC (2017–2019). However, the reference filter does not estimate parameters related to the gravity of Jupiter and the Galilean moons. These parameters were adopted into our Navigation OD, since they were found to have a non-negligible impact on the filter solution. The implemented setup estimates the following parameters:

- arc-wise spacecraft initial states $\mathbf{x}_{sc}(t_0^i)$, with base (*i.e.* nominal) *a priori* uncertainty of 15 km on each Cartesian position component and 10 cm/s on each Cartesian velocity component.
- arc-wise initial states of Galilean moons $\mathbf{x}_j(t_0^i)$ ($j = 1, 2, 3, 4$). The *base a priori* position uncertainty was taken at 15 km along the three TNW directions. Velocity uncertainty components of the *base a priori* were derived from the differences between IMCCE and JPL ephemerides NOE-5-2021[5] and JUP365[6], respectively.
- gravitational parameter μ and coefficients $C_{2,0}$ and $C_{2,2}$ of the spherical harmonics gravity field expansion of each Galilean moon, where the *a priori* uncertainties were adopted from Schubert et al. (2004).

---

[4] For the inversion of the right hand side, we scale the estimated parameters such that the partial derivatives in $\mathbf{H}$ are in the range $[-1, 1]$.

[5] https://ftp.imcce.fr/pub/ephem/satel/NOE/JUPITER/
[6] https://ssd.jpl.nasa.gov/sats/ephem/

- gravitational parameter μ and coefficients $C_{2,0}$, $C_{3,0}$ and $C_{4,0}$ of the spherical harmonics gravity field expansion of Jupiter, where the *a priori* uncertainties were taken from Notaro et al. (2021) for μ and Durante et al. (2020) for the zonal coefficients.
- empirical acceleration terms c_i (one constant entry per TNW component) on the spacecraft, estimated at a constant value per 10 day sub-arc, with *base a priori* set to 10^{-8} m· s^{-2}.

and the following parameters were introduced as consider parameters

- bias for range observables, with uncertainty fixed at 2 m.
- biases for ground station position, with uncertainty fixed at 0.3 m per axis.

The *a priori* covariance used to constrain the estimation on each given arc is composed of a section which is does not evolve over the course of the tour, and a section which reflects the knowledge improvements from previous estimations and therefore evolves over the course of the tour. The spacecraft state and empirical acceleration parameters belong to the first group; their *a priori* covariance is reset to the *base* values at each arc. The moon states and gravity parameters belong to the latter group. As time invariant parameters, the gravity parameters estimated on arc i can simply be used as *a priori* constraints on the following arc $i + 1$. As time variant parameters, the moon states covariance $\mathbf{P}_{qq}^i$ of arc i needs to be propagated in time to the beginning of arc $i+1$. There the propagated covariance is combined with the moon state *base* covariance and the result constitutes the *a priori* covariance of arc $i + 1$. This ensures that the *a priori* covariance at arc $i + 1$ benefits from the information contained in the previous arcs. The post-fit moon state covariance from arc i is thus first mapped to the initial epoch of the subsequent arc $i + 1$, using Eq. (10), to obtain the mapped covariance matrix $\mathbf{P}_m^{(i \to i+1)}$. However, $\mathbf{P}_m^{(i \to i+1)}$ may contain uncertainties higher than those of existing ephemeris solution (e.g NOE-5-2021). To account for this, the mapped covariance is combined with the *base* moon covariance (see above) $\mathbf{P}_m^{b, i+1}$ as follows:

$$\left(\mathbf{P}_{m,0}^{i+1} \right)^{-1} = \left(\mathbf{P}_m^{b, i+1} \right)^{-1} + \left(\mathbf{P}_m^{(i \to i+1)} \right)^{-1} \tag{11}$$

On the first arc $i=1$, the *a priori* strategy is initialised with the *base a priori* moon covariance $\mathbf{P}_{m,0}^1 = \mathbf{P}_m^{b, 1}$.

In the navigation operations of prior missions with multi-flyby tours of the Galilean moons (Galileo) and Saturnian moons (Cassini), empirical degrading of the propagated moon state knowledge was employed in the navigation filter. This is a conservative measure, in which the moon state covariance determined on arc i is increased by an empirical factor before it is passed on and used as *a priori* knowledge in the estimation of the following arc $i + 1$. This practice aims to compensate for the potential underpredictions of formal errors in the covariance and the model's capability to propagate these in time.

No such measures were implemented into the reference filter setup by ESOC (2017–2019), nor in our nominal model. Nonetheless, we added an empirical degrading scheme as optional setting into our filter and have examined the effect it has on the results presented hereafter. Since the relevance of this practice was found to be limited for our application, its implementation and effect on the moon state knowledge evolution are discussed in Appendix.

3. Methodology (II) — GNC operations and statistical ΔV

This section addresses the second block (see Fig. 2) of the analysis setup: the computation of the ΔV expense for corrective manoeuvres.

Section 3.1 discusses relevant Guidance, Navigation and Control (GNC) aspects, focusing on the interplay of Navigation OD and guidance schemes.

The design and computation of trajectory correction manoeuvres (TCMs) is addressed in Section 3.2. Section 3.3 gives a more detailed introduction to the concept of statistical ΔV budgets and describes how they are computed in this study.

3.1. GNC operations

During the mission, TCMs are required to ensure the pre-defined trajectory is flown (within a range of uncertainty). Fig. 3 shows a typical guidance strategy for a JUICE satellite flyby arc, using a "targeting" and "pre-encounter" (p/e) TCM to reduce flyby target misses and a "clean-up" (c/u) TCM to correct trajectory errors downstream of the flyby. The JUICE mission adopts this common guidance strategy, placing the p/e and c/u manoeuvres 3 days before (upstream) and after (downstream) closest approach (c/a), respectively (ESOC, 2017–2019).

While the targeting manoeuvre at the beginning of the flyby arc (apojove) is oftentimes combined with a deterministic orbit trim manoeuvre, p/e and c/u manoeuvres are typically purely stochastic manoeuvres, with an expected vectorial magnitude of $\mathbf{0}$. Their design is only driven by the stochastic deviation of the spacecraft state w.r.t. its nominal trajectory, an estimate of which is provided by the navigation operations. The need for such stochastic manoeuvres is accounted for in the so-called statistical ΔV budget (see Section 3.3).

Using a navigation OD setup (Section 2), a best estimate $\hat{\mathbf{q}}$ and associated covariance $\mathbf{P}_{qq}$ (Section 2.2) of all relevant system parameters is computed, which is then used for TCM design. In the case of the JUICE mission, the generation of OD solutions for p/e and c/u manoeuvre design uses a nominal data cut-off (DCO) 2 days prior to the given manoeuvre (*i.e.* no tracking data newer than two days before the manoeuvre is used for the design of the manoeuvre).

In the simple, exact targeting strategy that is adopted in this analysis (see Section 3.2), each TCM is designed such that the estimated trajectory error (difference between a reference target point $\mathbf{B}$ and the current best estimate of the spacecraft state at the epoch) is eliminated. However, the uncertainty of the spacecraft state estimate on which the TCM design is based, is not eliminated — it is merely "re-centred" on the nominal condition $\mathbf{B}$. The uncertainty will evolve alongside the system evolution and will manifest itself in subsequent spacecraft state estimates as the "new" error (trajectory dispersion), which is to be corrected by the following manoeuvre. This approach does not account for the dispersion due to manoeuvre execution errors, because they are not included in the set of estimated parameters $\mathbf{q}$. This is acceptable for our analysis, because the execution error induced ΔV cost is only sensitive to moon state knowledge to second order and is thus not expected to have a significant impact on the comparative ΔV analysis.

Moon ephemerides of improved accuracy will positively affect the general GNC operations, reducing flyby misses and the expense of statistical manoeuvres throughout the arc (e.g. Murrow and Jacobson, 1988; Ionasescu et al., 2014). However, it should be noted that moon ephemeris uncertainties contribute most strongly to dispersions downstream of the flyby: during close encounter the moon position error introduces significant deviations to the spacecraft dynamics, which results in amplified deviations from the reference trajectory when propagated downstream. Consequently, moon ephemeris improvements will predominantly affect the clean-up manoeuvre downstream of the flyby. Since these manoeuvres also contribute most heavily to the statistical ΔV budget (ESOC, 2017–2019), they are expected to yield the biggest ΔV savings with the proposed ephemeris update strategy. Because this study wants to investigate whether a ΔV budget reduction is possible, it was decided to first investigate manoeuvres which are most affected by the moon ephemeris error source and to omit the influence of the less sensitive targeting and pre-encounter TCMs.

3.2. Corrective manoeuvre design

Various TCM targeting strategies exist (D'Amario et al., 1981; Wolf and Smith, 1995; Buffington et al., 2005), in which the next-body B-plane targeting (*e.g.* Cho et al., 2012) is a common option. It prescribes that every TCM targets the reference conditions of the upcoming flyby, mapped onto the B-plane of the flyby body. In some cases, this can give
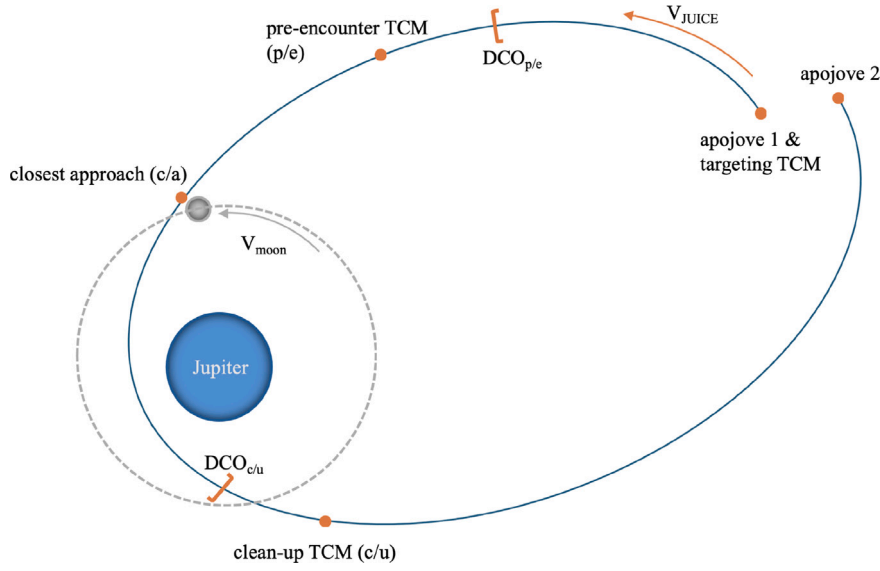
Fig. 3. Typical three-manoeuvre guidance scheme for flyby arcs. DCO denotes the Data Cut-off for the design of the subsequent manoeuvre. The "targeting" TCM, typically at apojove, is not relevant for this analysis and therefore omitted from the figure.

rise to large c/u manoeuvres, in which case targeting the reference position at upcoming apoapsis is a suitable alternative (ESOC, 2017–2019). Advanced targeting strategies, such as the ones used by ESOC (2017–2019) use optimisation algorithms over multiple arcs and (biased) flyby targets, which is not considered necessary for our comparative analysis. Instead, a simple targeting strategy is chosen, in which c/u manoeuvres target the reference position at upcoming apoapsis.

Our computation of the TCM manoeuvres is based on the numerical propagation of the JUICE-Jovian system dynamics and its covariance, which was introduced in Section 2.1, where we model manoeuvres as perfectly instantaneous changes of the spacecraft velocity as follows.

We use $\boldsymbol{\Delta X}(t_{c/u})$ and $\boldsymbol{\Delta X}(t_{apo})$ to denote the estimated trajectory errors (*i.e.* expected amplitude of deviation of estimated spacecraft trajectory from the reference trajectory), at the time of the cleanup manoeuvre and at apoapsis.

Assuming linear behaviour, the error at the time of the cleanup manoeuvre can be mapped to the apoapsis time by use of the state transition matrix $\boldsymbol{\Phi}$ (Eq. (2)):

$$\boldsymbol{\Delta X}(t_{apo}) = \boldsymbol{\Phi}\left(t_{apo}, t_{c/u}\right)\boldsymbol{\Delta X}(t_{c/u}) \tag{12}$$

A single instantaneous ΔV change cannot be used to target a full (six-component) spacecraft state; the chosen scheme targets the reference *position* ($\mathbf{x}$ at apoapsis. The manoeuvre design only considers the position components $\boldsymbol{\Delta x}(t_{c/u})$ of the residual spacecraft trajectory error at target epoch.

$$\boldsymbol{\Delta V} = \boldsymbol{\Phi}_{\partial v/\partial x}\left(t_{apo}, t_{c/u}\right)^{-1}\boldsymbol{\Delta x}(t_{apo}) \tag{13}$$

We note that the implemented manoeuvre computation algorithm as described above does not provide any means to constrain the velocity error components $\boldsymbol{\Delta v}(t_{apo})$ at the target. Post-correction velocity residuals were monitored and comparison with the pre-correction velocity errors shows that the position-targeting scheme has the natural tendency to mitigate deviations in the velocity components, too. It is thus concluded that this limitation does not impose any unintended stress on the downstream spacecraft guidance and the unmodelled contributions to the statistical ΔV budget (*i.e.* targeting, pre-encounter TCMs).

3.3. Statistical ΔV budgets

Statistical ΔV analyses are performed in order to allocate sufficient resources to the performance of statistical TCMs. Its main outputs are

the expected value and 99th percentile of the mission's statistical ΔV expense. The most common method used for computing statistical ΔV budgets (*e.g.* Raofi et al., 2000; Weeks, 2008; Martin-Mur et al., 2014) and which is adopted for this work, is the Monte-Carlo (MC) analysis.

For the MC analysis, trajectory errors are simulated by drawing statistically representative samples of the spacecraft dispersion, and a corrective manoeuvre is designed for each. The manoeuvre cost (ΔV) is stored for the correction of all dispersion samples. For a large enough amount of MC samples, the resulting population of ΔV values is representative of the TCMs' statistical ΔV expense, which can thus be characterised using the statistical properties of the ΔV population.

Recalling (from Section 3.1) the connection between spacecraft state uncertainty during TCM design and dispersion downstream of that manoeuvre, an algorithm for the creation of dispersion samples can be defined. This algorithm, applied to generating dispersion samples for the computation of the clean-up TCM, is presented below. Note that the comparative nature of the analysis allowed us to decouple the GNC operations of the individual flyby arcs, such that the following algorithm can be applied to the c/u manoeuvre of each flyby-arc independently.

1. The uncertainty of the system state estimate at p/e design, which is based on data cut-off time $DCO_{p/e}$, is propagated to c/u manoeuvre time. Using the propagation method given by Eq. (10), the covariance matrix

$$\mathbf{P}_{yy}^{(t_0 \to t_{c/u})}\left(DCO_{p/e}\right) \tag{14}$$

is obtained.

2. The spacecraft state covariance matrix given in Eq. (14) constitutes the trajectory dispersion at c/u, which arises from spacecraft and flyby body uncertainties in the OD solution of the p/e data cut-off. Note that it does not account for the execution error contribution of the p/e manoeuvre (see Section 3.1). The estimate of the trajectory dispersion at c/u is itself affected by OD uncertainties, but under the assumption that OD errors are small compared to the trajectory dispersion (as reported by e.g. Boone et al., 2017; Bellerose et al., 2016), and that OD contributions do not substantially alter the statistics of the estimated trajectory error, this can be neglected.

3. We use $\boldsymbol{\Sigma}$ to denote the spacecraft state portion of Eq. (14), such that the estimated trajectory dispersion at c/u manoeuvre time can be modelled using a multi-variate normal distribution

$$S \sim N_6(\mathbf{0}, \boldsymbol{\Sigma}) \tag{15}$$

from which 100000 samples $\bar{S}$ are drawn.

4. Each dispersion sample $\bar{S}$ is fed into the TCM design algorithm, where – under the previously introduced assumptions – it represents the estimated trajectory error at manoeuvre time $\Delta\mathbf{X}(t_{c/u})$. A corrective manoeuvre is computed and its ΔV cost is stored.

5. The resulting ΔV population is considered representative of the statistical ΔV budget for the c/u manoeuvre on the given flyby-arc. We reduce these distributions to statistical parameters (mean, 99th percentile), which will then be used to characterise the ΔV population.

4. Methodology (III) — External Ephemeris products

In Section 4.1, selected characteristics of science OD setups are discussed and differences w.r.t. the Navigation OD are highlighted. The coupled estimation by Fayolle et al. (2022) is adopted as a source of data for science ephemerides from JUICE. Section 4.2 discusses methods with which moon ephemerides from radio science data can be integrated into the Navigation OD in the form of external ephemeris updates and shows how such updates are simulated in the navigation OD framework (see Fig. 2).

4.1. Science ephemeris generation from JUICE

Recent publications on ephemeris generation from JUICE data have adopted a coupled estimation (*e.g.* Dirkx et al., 2018; Lari and Milani, 2019; Fayolle et al., 2022), which differs from the strictly arc-wise setup of the Navigation OD (see Section 2.4). The method directly estimates single-arc initial states of the moons and multi-arc initial states of the spacecraft, in a single inversion, as opposed to the arc-wise spacecraft and moons estimation of the Navigation OD.

Although theoretically more realistic, there are challenges to overcome in applying the coupled method for ephemeris estimation. In particular, it imposes challenging requirements on the accuracy and consistency of the dynamical models, over both short and long timescales. This makes it a poor choice for navigation operations, where fast results are essential.

For their ephemeris solution, Fayolle et al. (2022) simulate 3GM radiometric range observables with a noise level and range bias of 0.2 m and 0.25 m respectively, and a cadence of 1 h; Doppler measurements with a noise level of 15 μm/s at an integration time of 60 s. For this study, we do not consider VLBI data from PRIDE for our radio science solution, as the post-processing procedures to obtain the data from raw observation requires a longer lead time, which is not compatible with the relatively fast turnaround time required for our analysis. The comparison in Table 1 shows that these characteristics differ substantially from the tracking data for navigational purposes.

The science setup also employs a more sophisticated dynamical model than the navigation OD setup (Section 2.1). Most notably, it models the gravity fields of the Galilean moons at greater detail and accounts for tidal dissipation in Jupiter and the satellites. More importantly, it includes more estimated parameters, such as higher-degree gravity field coefficients, into the estimation.

4.2. External ephemeris products in GNC operations

It is worth noting that there are certain operational aspects that complicate the use of external ephemeris products in the Navigation OD. The Navigation OD is an essential part of a strict operational GNC framework. Spacecraft tracking data is made available to the Navigation OD on the shortest route possible. From there, OD solutions must be generated within less than a day to enable a timely design and processing of subsequent TCM commands (Section 3.1). As a result, Navigation OD solutions have a data cut-off lag of less than a day,

Table 1

Comparison of the radiometric measurements used in navigation and science OD. Note that when scaling navigation Doppler data to 60s integration time for direct comparison with the science data, the resulting noise level at 620 μm/s is substantially worse than the 15 μm/s of the science data.

	Navigation OD	Science OD
Instrument	Nav subsystem	3GM
Coverage	full-arc	c/a ± 4 h
	range | Doppler	range | Doppler
Cadence	1 h | 1 h	1 h | 60 s
Noise	10 m | 80 μm/s	0.2 m | 15 μm/s

(2 days w.r.t. execution of associated manoeuvre). Scientific ephemeris products on the other hand are typically produced with a longer delay, to ensure that analysis procedures for the data at hand are optimised. . Here, the number of flybys by which the analysis is delayed is the relevant figure of merit, which will hereafter be indicated by ℓ. In using scientific ephemeris products into navigation operations, it is therefor crucial to keep ℓ as short as possible. This will be challenging during the beginning of the mission in particular, when there has been little opportunity to characterise analysis procedures in sufficient detail.

In our analysis, the Navigation OD framework takes simulated moon ephemeris updates from external ephemeris products as input (see Fig. 2). The ephemeris update method uses the external moon ephemeris as an *a priori* covariance for regularising the estimation of the moon initial states on the given arc (Boone et al., 2017).

To calculate the influence of this procedure on the Navigation OD covariances, we modify the covariance used as input to Eq. (11), which then becomes

$$\left(\mathbf{P}_{m,0}^{i+1}\right)^{-1} = \left(\mathbf{P}_m^{b,i+1}\right)^{-1} + \left(\boldsymbol{\mathcal{P}}_m^{(i-\ell)\to i+1}\right)^{-1} \quad (16)$$

where $\boldsymbol{\mathcal{P}}_m^{(i-\ell)\to i+1}$ is the covariance matrix associated with the external moon *a priori* information $_m^{(i-\ell)\to i+1}$, produced with a delay of ℓ flybys.

5. Results & discussion

Using the setup shown in Fig. 2 and the settings described in Section 2, we have simulated the estimation of Galilean moon ephemerides from radiometric navigation data during the JUICE multi-flyby tour.

Section 5.1 presents and discusses the results obtained from the Navigation OD. Using the external moon ephemeris interface, a comparative analysis on the statistical ΔV cost with and without moon ephemeris updates was performed, the results of which are presented in Section 5.2. Lastly, the insights that were gained from comparing the characteristics of navigation and science tracking data, as well as the respective ephemeris products, are used to discuss some potentially more interesting ideas for data synergy in Section 5.3.

Despite being derived on the basis of the superseded CReMA 3.2, the results and conclusions presented hereafter are expected to have a high degree of relevance for the current and future mission profiles (see Section 2).

5.1. Navigation OD — uncertainty evolution

Fig. 4 shows the formal error evolution from the Navigation filter for each estimated body over the course of the whole flyby tour. The formal errors are given in the TNW components, where T is the along-track direction, N is the direction normal to the track and W is the cross-track direction.

The uncertainty of the JUICE trajectory w.r.t. Jupiter, shown in Figs. 4a, varies greatly within the course of each arc. Starting at comparatively large uncertainty at apojove (where each of our estimation arcs start), the spacecraft state is much better constrained around the point of closest approach.
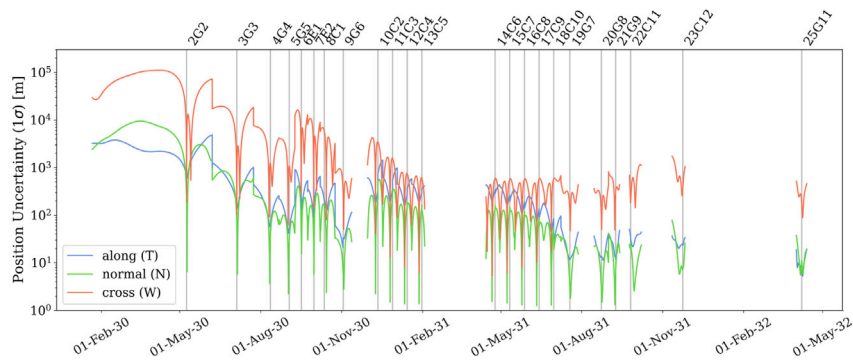
(a) Uncertainty evolution of JUICE position w.r.t. Jupiter. The discontinuous jumps at the beginning of each flyby arc are a direct consequence of the *a priori* strategy (see section 2.4), which re-sets the spacecraft *a priori* to its base value for each arc-wise estimation.
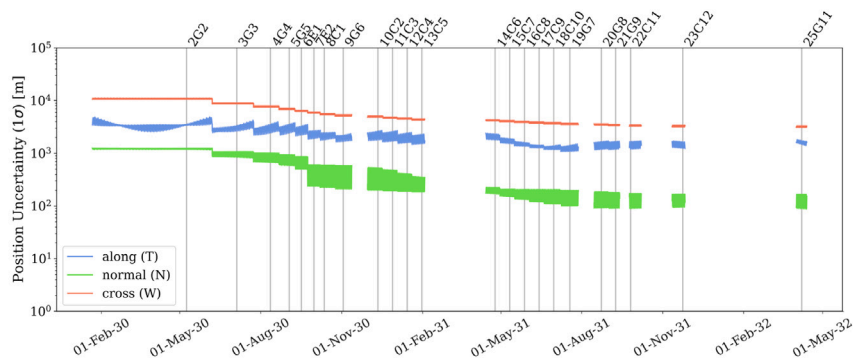
(b) Uncertainty evolution of Io position.
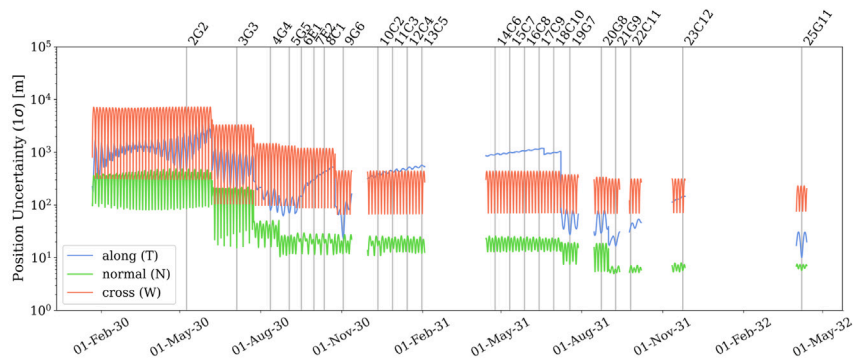
(c) Uncertainty evolution of Europa position.

Fig. 4. Knowledge evolution of the JUICE-Jovian system, as computed by the Navigation OD setup in baseline configuration. Vertical lines mark the time of moon encounter on each considered arc.

Despite the *a priori* covariance being reset at the beginning of each arc for the spacecraft state, one can also observe an ongoing improvement of JUICE state knowledge w.r.t. Jupiter over the course of the tour. This is the effect of the improving moon state uncertainty evolution over the course of the tour: the improved knowledge of the flyby moon state translates into an improved trajectory estimate of the spacecraft.

Studying the state uncertainty evolution of the Galilean moons (Figs. 4b to 4e) over the course of the multi-flyby tour and especially during its early/mid mission stage (up to and including flyby 13C5), one can see the effect that close encounters have on the coupling of spacecraft tracking data and the encountered moon — the overall moon knowledge can be inferred much better from the spacecraft tracking data after close encounters.

The two in-plane components of the moons' positions (radial and along-track) show very different behaviour from one another. When propagating the dynamics forward in time, a radial position error will spill over into downstream along-track deviations that grow with the
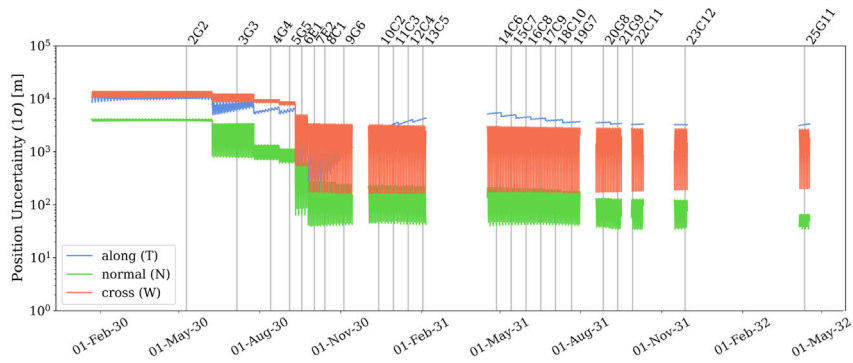
(d) Uncertainty evolution of Ganymede position.
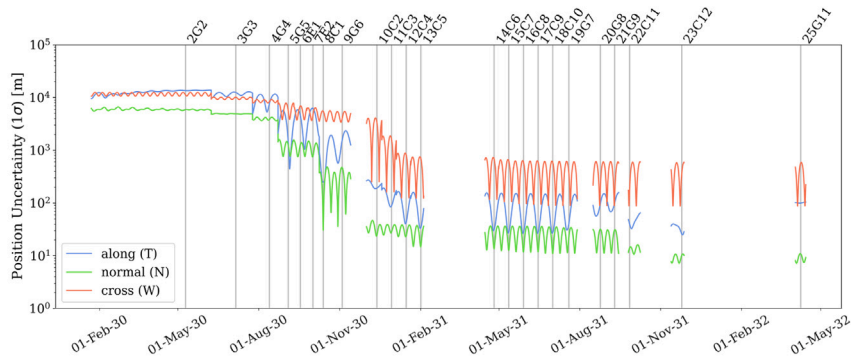
(e) Uncertainty evolution of Callisto position.

Fig. 4. (*continued*).

propagation duration. The radial components are therefore much more easily constrained, which is reflected in the low levels of the associated uncertainties throughout Figs. 4b to 4e. Conversely, the along-track uncertainty is thus much more prone to secular increase from system propagation, which can be observed in *e.g.* Figs. 4c and 4d.

Furthermore, the in-plane resonance of the three inner Galilean moons makes the in-plane state components sensitive to spacecraft flybys of any other moon in resonance. These create indirect couplings of the spacecraft dynamics and the given moon, via the flyby body. This mechanism is adequately captured in the implemented Navigation OD, as can be seen by comparing how the uncertainties of Io (Fig. 4b) and Europa (Fig. 4c) state components respond to flybys 3G3, 4G4, 5G5 of Ganymede (in resonance) and flybys 8C1, 10C2, 11C3 of Callisto (not in resonance).

As a result of this mechanism, the state knowledge of Io is improved, especially in-plane, without any direct observations or flybys. The improvement is smaller than that shown in ESOC (2017–2019), where direct observations of Io via OpNavs constrain the moon state even further. Another feature that is linked to (the absence of) indirect coupling with the spacecraft dynamics, can be seen in the along-track knowledge evolution of Europa during the sequence of 9 subsequent Callisto flybys. This constitutes a prolonged lack of direct or indirect spacecraft coupling with Europa, which results in a dramatic degrading of the along-track components. Similar observations can be made for Ganymede.

Overall, it is also worth highlighting the rapid improvements of the moon state knowledge, compared to the *a priori* information, from direct coupling and the implications for the navigation of subsequent flybys. In the first arc alone (2G2), post-fit uncertainty of Ganymede is reduced by almost to two orders of magnitude (post-fit of $\sim$ 200 m in the radial direction). For later Ganymede flybys (20G8, 21G9), in-plane position knowledge is consistently in the order of tens of meters, while

the cross components are in the order of hundreds. Similar observations can be made for Callisto, where comparable uncertainty levels are reached after the first series of flybys (10C2-13C5) and stay in effect over the course of the remaining ten Callisto flybys.

Due to the low cadence of measurements during close encounters, it cannot be expected that the navigation tracking data is able to resolve the gravity field of the encountered bodies to greater extend that prior missions. Indeed, it was found that the navigation filter cannot improve upon the *a priori* knowledge of gravity-related parameters. Including the gravity parameters into the filter does however affect the quality of the estimated moon state knowledge: the estimation of the in-plane components of the flyby moons Europa, Ganymede and Callisto degrade by factor 3–5, where the radial component deteriorates most significantly. The radial component of Europa is most affected. In Fig. 4c it converges to a formal error of $\sim$ 100 m, while without the estimation of gravity parameters the formal error would reduce to $\sim$ 20 m by the end of the tour.

From the discussion of the produced OD solutions, it can be concluded that the uncertainty evolution shows behaviour expected of the JUICE flyby tour of the Galilean satellites, showing features that will be important in our subsequent discussion. Additionally, the implemented OD is qualitatively consistent and quantitatively comparable with that of ESOC (2017–2019).

5.2. ΔV savings from external ephemeris updates

This section presents the findings of the comparative statistical *ΔV* analysis, which quantifies the potential for *ΔV* savings from external moon ephemeris updates. Section 5.2.1 investigates an idealised case with perfect moon ephemerides, while Section 5.2.2 approximates an operational scenario using moon ephemerides from the external source. Lastly, Section 5.2.3 suggests an alternative strategy for achieving *ΔV* savings.

Table 2

ΔV savings on the c/u manoeuvre – effectuated by perfect moon knowledge and idealised external ephemeris updates – next to the total statistical ΔV allocation for clean-up manoeuvres and the cost of the GCO-200 phase. Relative savings from Fig. 5 were translated to absolute savings by applying them to the statistical ΔV allocations reported in the JUICE navigational analysis (ESOC, 2017–2019). This method is not fully consistent, but the resulting numbers can indicate how the maximum attainable savings from moon ephemeris updates relate to the total statistical ΔV budget and the cost of mission extension.

	ΔV savings - 99% limit case	ΔV savings - 99% science ephemeris updates	ΔV allocation (c/u) - 99% (ESOC, 2017–2019)	Cost of GCO-200 (ESA, 2014)
relative savings	7.8%	0.64%	130.5 m/s	~ 90 m/s
absolute savings	10.2 m/s	0.83 m/s		
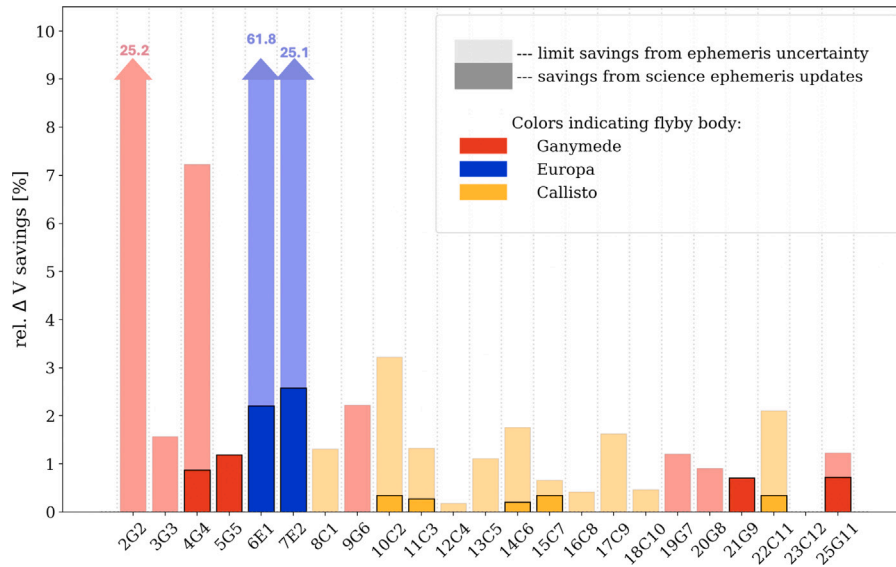
Fig. 5. ΔV savings on the c/u manoeuvre for each arc, showing the potential savings from perfect moon knowledge and the fraction which can be effectuated by science ephemeris updates. Arc 23C12 was excluded, because the post-flyby section of the arc is too short to accommodate the generic guidance scheme.

5.2.1. Limit case: Perfect ephemeris updates

Before involving the specific radio science ephemerides from Fayolle et al. (2022) into the analysis, it was explored to what extent generic moon ephemeris improvements can be advantageous for the statistical ΔV expense of the clean-up manoeuvres. This was done by considering the limit case, in which the Navigation OD is given perfect moon state knowledge at the start of every arc. Based on the resulting OD solution, the statistical ΔV cost was computed for the c/u manoeuvres and compared to the costs associated with the baseline navigation solution.

By inspecting Fig. 5, which sketches out the potential savings on each arc, it can be seen that the moon ephemeris error only acts as a ΔV-driving factor during the early tour, specifically when Ganymede and Europa are encountered for the first and – in the case of Europa – second time. For these arcs the relative ΔV-saving potential was found to be substantial. These arcs are also where the largest ΔV allocation for c/u manoeuvres are reported (ESOC, 2017–2019). On later flyby arcs, the saving potential is in the domain of single-digit percentages and reported ΔV allocations are smaller. It must thus be concluded that the Navigation OD constrains the moon state uncertainties so rapidly, that they effectively do no longer drive the c/u manoeuvre cost significantly for the remainder of the tour. Instead the ΔV budget appears to be almost entirely driven by the spacecraft state uncertainty. While the spacecraft orbit uncertainty also decreases with the improved moon knowledge, there are other factors such as the noise on the tracking data, stochastic accelerations and systematic error sources (captured by the consider parameters), that impose a moon-independent limit on the quality of the spacecraft trajectory determination.

The resulting numbers in Table 2 effectively indicate the theoretical limit which could be achieved by implementing external moon ephemerides, which amount to 10.2 m/s w.r.t. the baseline navigation solution. Although this will not be a significant game-changer for

JUICE, it would free up (in this limit case) more than 10% of the propellant required for a GCO-200 orbit.

As stated in Section 3.1, it is expected that other statistical ΔV allocations (for e.g. targeting and pre-encounter manoeuvres) will also benefit from better moon state knowledge, but are far less sensitive to the ephemeris updates than the examined c/u manoeuvres. But even if the ΔV savings on these manoeuvres were comparable to that of the c/u, their effect would not weigh in substantially due to their relatively small contribution to the overall ΔV allocation. Other beneficial effects on GNC performance, such as the reduction of the flyby target miss, have not been examined.

It should be noted this analysis was conducted without empirically degrading of transferred moon state knowledge, which was introduced in Section 2.4. With the degradation scheme, which naturally increases the formal errors on the moon states Appendix and the uncertainties in the spacecraft navigation, the statistical manoeuvre sizes increase and associated savings potential through perfect moon knowledge would increase. For the reasons mentioned in Appendix, the increased savings potential cannot be effectuated through updates from external ephemerides, which is why the degrading scheme is not included into the comparative ΔV study.

5.2.2. Operational: "radio-science-enhanced" navigation

For the external moon ephemerides, we use results from Fayolle et al. (2022), which rely exclusively on radio science data. Fig. 6 shows the average moon state uncertainties in the external ephemerides over the early stages of the tour next to the generally smaller uncertainties from the Navigation OD. During the early mission phase in particular, the Navigation OD solution shows significantly faster reduction in moon position uncertainty. Given that the external ephemeris solution is based on the more accurate radio science data, this is a counter-intuitive result, which is further investigated in Section 5.3.
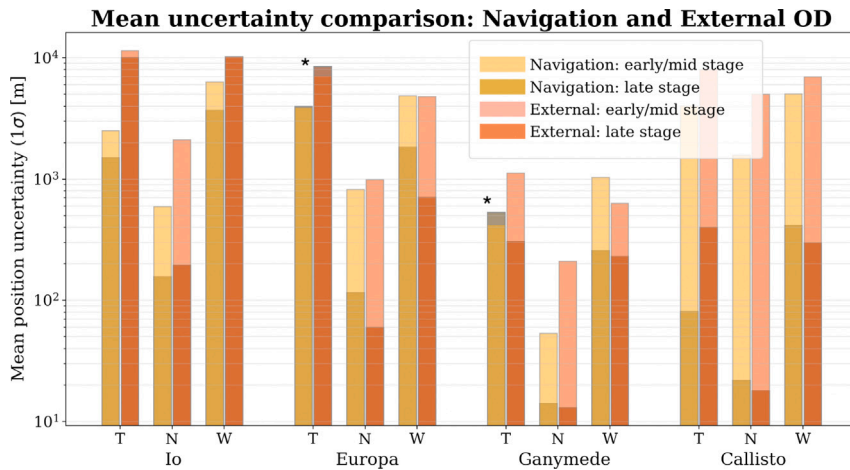
Fig. 6. Average position uncertainty over early/mid and late mission stages, comparing post-arc uncertainty levels of the External and Navigation OD. It can be seen that – with few exceptions – the external ephemeris cannot match the early/mid stage levels of the Navigation OD. Late stage uncertainty levels of the multi-flyby bodies Ganymede and Callisto become comparable between Navigation OD and External OD, with noticeable advantages for the External OD on the N- and W-components of the flyby moons Europa, Ganymede and Callisto. Early/mid mission stage is defined up to (and including) arc 13C5..

Recalling the observations from the theoretical limit case (Fig. 5), which showed that it is only during the early stages that moon state knowledge improvement can effectuate significant ΔV savings, it can be concluded that a 'radio-science-enhanced' navigation with moon knowledge updates from Fayolle et al. (2022) ephemerides is not an effective way to save statistical ΔV.

Despite this insight, a 'radio-science-enhanced' navigation was simulated and the associated ΔV cost was computed. Even though the operational time-lag ℓ (Eq. (11)) was neglected for this calculation, it confirmed that the 'radio-science-enhancement' is not able to significantly tap into the potential savings (Fig. 5). Total savings over all considered c/u manoeuvres amount to 0.78 m/s, which is 0.6% of the total ΔV allocation for c/u manoeuvres. Since these are very minor savings, which occur during the late phase of the mission, where expected cleanup manoeuvres are smaller, this indicates a negative result: nominal radio-science ephemerides from JUICE data cannot be a suitable method to reduce the JUICE mission's propellant expenditure during the flyby tour.

5.2.3. Ephemeris updates prior to mission

Instead of in-mission ephemeris updates, a more effective way to tap into the ΔV savings outlined by the theoretical limit (Table 2) is to improve the Galilean moon ephemerides before the onset of the JUICE flyby tour. This requires the use of data sources independent of the JUICE mission, such as ground-based astrometric measurements of mutual events (Arlot and Emelyanov, 2019), mutual approximations (Fayolle et al., 2021) and stellar occultations (Morgado et al., 2019), but also the Europa Clipper mission, which is scheduled to arrive in the Jovian system before JUICE (Tarzi et al., 2019; Magnanini et al., 2024). By the time of JUICE's first encounters with the Galilean moons, Clipper is expected to have collected more than one year's worth of data in the Jovian system. Since this mission is focused on acquiring data for the detailed characterisation of Europa (Verma and Margot, 2018), its consideration may be especially useful for effectuating ΔV savings during JUICE's Europa flybys in particular (Fig. 5, blue bars). Analyses, which quantify the expected extent of such pre-arrival improvements, are to be carried out in preparation of the JUICE mission.

5.3. Further data synergy

In Sections 5.1 and 5.2 it was shown that the Navigation OD solution constrains moon state knowledge more rapidly than is expected for radio-science-based OD solutions from *e.g.* Fayolle et al. (2022).

It was found that the crucial point, which eventually creates the early-mission advantage for the navigation data set, is the temporal and spatial distribution of the observations. By visualising the design matrix **H** (recall Eqs. (5) and (7)) on arc 2G2 in Fig. 7, it can be seen that for spacecraft and flyby body (Ganymede) there is a very sharp gradient in the partials between pre- and post-encounter observations. This visualises the fact that observations made both during and after the encounter of the flyby moon are extremely valuable for the estimation of the spacecraft and flyby body states. The specific behaviour of the entries in this matrix is a result of the fact that the estimated initial states are defined far upstream the arc. However, regardless of the point along the arc where the state is estimated, a sharp gradient will be seen at closest approach. More generally speaking, it is the distribution of the tracking observations, extending far from the reference epoch at which the initial state is defined, which enables the navigation filter to constrain spacecraft and moon ephemerides so well, especially during these long tracking arcs.

Fig. 7 furthermore shows that the observations relate to Europa's state in a similar way than they relate to spacecraft and the flyby body itself — namely with a steep gradient over the closest approach. This reveals the mechanism underlying the "co-evolution" of the dynamically coupled moons, that was previously observed in Fig. 4 and discussed in Section 5.1: improvements of the flyby moon ephemeris translate into the dynamically coupled bodies in the system.

By closer inspection of Fig. 7, and specifically the information content on Io, it can be seen that pre-flyby observations contribute more strongly to the estimation than is the case for other bodies. This indicates that the tracked spacecraft picks up the dynamical signature of Io prior to any close encounters. The surprising result is demonstrated more clearly by Fig. 8. It shows that the isolated pre-encounter (up to 3 days before encounter) data are capable of constraining the Io state knowledge far beyond the *a priori* values. Adding the (post-) encounter data to the inversion contributes a comparatively little reduction in the Io formal errors.

The previous paragraphs discuss the full-arc coverage and the volume of observations far up- and downstream of the close encounter as a potentially powerful asset of the navigation data set. It not only allows for precise estimation of spacecraft and flyby body, but through its perturbation on the spacecraft, the data also seems to be sensitive to the direct dynamical signatures of Io at a level below its a priori knowledge. However, it must be recalled that this notion relies on the results of a covariance analysis, in which dynamical and observational models are idealised (Section 2.2). Because simulated tracking data is perfectly consistent with the dynamical model in our analysis, it can
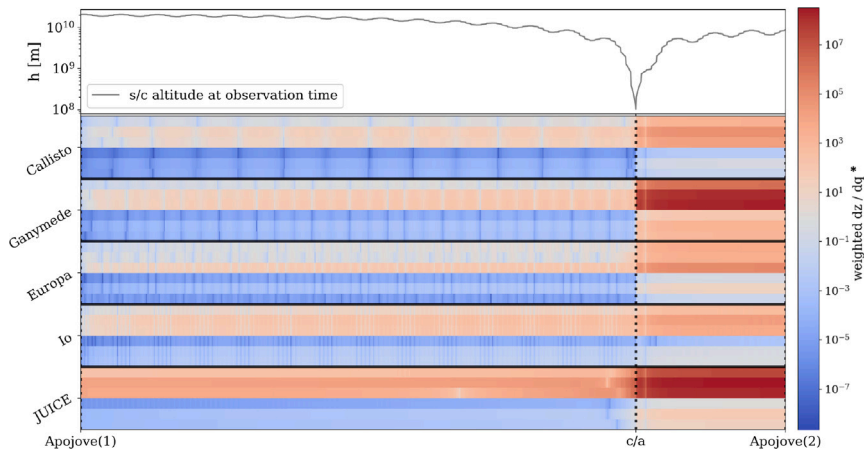
Fig. 7. Weighted design matrix ($\mathbf{H}^T$) of arc 2G2: the *x*-axis is the dimension of the observation timeline, shown from start to end of the given arc, the *y*-axis the dimension of the estimatable state parameters. Each entry of the design matrix relates a given observation z to an estimatable parameter q, via the partial derivative $\partial z/\partial q$. The magnitude of these partials indicate how influential a given observation is for constraining the knowledge of the associated parameter. The additional axis on top of the figure indicates how distant the object of measurement (spacecraft) is from the flyby body for any given observation. Note that the design matrix in this figure has been reduced to contain range-rate entries only. * The units of the partials are [1/m] for position (upper three) components and [s/m] for the velocity (lower three) components of each body's state.
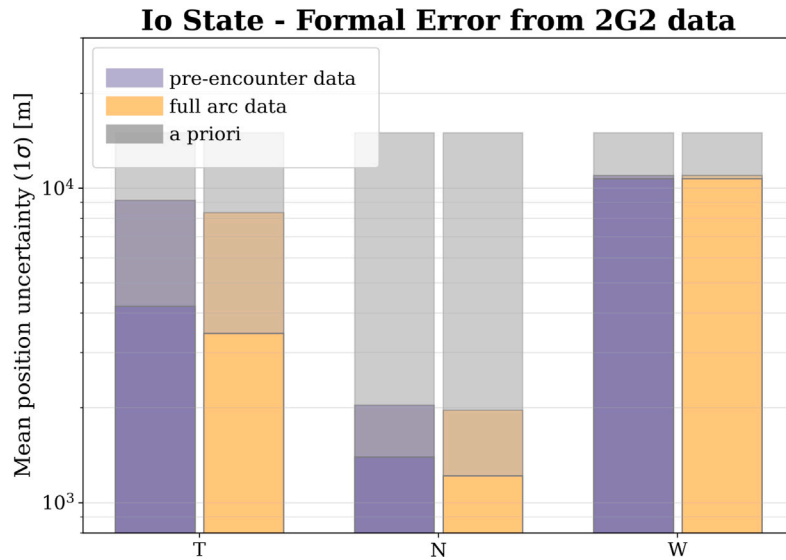
Fig. 8. Mean formal error of Io state, estimated from isolated pre-encounter data and from the full 2G2 data arc. The full colours show the results from the baseline navigation filter, while the muted colours are obtained by decreasing the empirical acceleration averaging time to a more conservative 10 h. While the shorter averaging degrades the solution, especially in the along-track (T) direction, it can be seen that for both cases the majority of the improvement w.r.t. the *a priori* is enabled by the pre-encounter observations, while the (post-) encounter observations only contribute a small additional reduction.

in theory be inverted in large batches spanning long timescales. In practice, this inversion is limited to observation batches over timescales for which the dynamical model is sufficiently consistent. While it will likely be possible to define a dynamical model that is sufficiently consistent over the manoeuvre-free 8 h radio science tracking arcs around closes approach, mismodelling of the dynamics (and in particular of non-conservative accelerations acting on the spacecraft) will show significantly over the month-long navigation tracking arcs of the early tour.

In the context of a covariance analysis, one way to assess the impact of such dynamical mismodelling is by solving for or considering additional parameters that represent this, which will typically degrade the formal uncertainties obtained for the spacecraft and moons states.

Firstly, to study the effect of the manoeuvre errors on the filter solution on the long first arcs, we use the manoeuvre size and error models from ESOC (2017–2019) and implement them as consider parameters into the filter. This preliminary evaluation showed that even as consider parameters the manoeuvre execution errors do not degrade the quality

or stability solution substantially with respect to the results presented in this manuscript.

The sum of other mismodelling effects related to *e.g.* solar radiation pressure coefficients, accelerometer calibration errors, *etc.* may have a more detrimental impact on the long tracking arcs. To address this, we rerun our analysis with the estimation of empirical accelerations over a more conservative averaging window of 10 h (which is a more typical value for such navigation applications). When doing so, the estimation of the Io state from the 2G2 arc degrades by a factor 2 in the along-track (T) and factor 1.5 in the radial (N) direction (Fig. 8). The same figure shows that despite the more conservative modelling of the empirical accelerations, the majority of Io state knowledge can be retrieved from the pre-encounter dynamics of the s/c.

However, the large number of estimated empirical acceleration parameters cause the inversion on the long arcs (2G2, 3G3) to become unstable, in the sense that covariance becomes (nearly) non-invertible. Although this does not directly impact the formal errors for Io in our analysis, it does highlight a substantial practical problem that will need

to be overcome, if indeed the JUICE navigation data is to be used over long arcs to improve the constraints on Io's state. One solution would be to break up the long arcs into smaller ones, but this will reduce the advantageous effects of long navigation data coverage. Another possibility would be to improve the a priori constraints on the moons before the first flyby. This may be achieved in a number of ways, for instance using the first sets of tracking data of Europa Clipper (which will arrive in the Jupiter system about a year and a half before JUICE), or high-accuracy Earth-based observations such as mutual approximations (Fayolle et al., 2021) or stellar occultations (Morgado et al., 2019; Fayolle et al., 2023a).[7]

In addition, high-accuracy dynamical modelling of the moons themselves will also be essential for our propagated covariances to be a realistic quantification of the navigation data's contribution. However, considering the exceptionally small post-mission ephemeris uncertainties that could be achieved (Fayolle et al., 2022), improving dynamical modelling quality of the moons is a known challenge that will have to be tackled for the mission's science objectives to be realised (Van Hoolst et al., 2024). To quantify the need for this in the context of our work, we show in Appendix the results of an analysis where we degrade the post-flyby covariance propagation, to account for errors in the moon dynamical modelling, which indeed shows a moderate worsening of the moon position covariance.

Due to these reasons, our results indicate an interesting potential synergy between science data and navigation data for improving the Galilean satellite ephemerides, but also highlight a number of significant challenges that will need to be overcome to realise this synergy. Most notably, the accurate dynamical modelling of the JUICE spacecraft will need to done over a long arc, with a limitation on the number of correction parameters (such as empirical accelerations) to prevent instability in the solution. Recent efforts in non-conservative force modelling for the BepiColombo spacecraft have shown an impressive level of attainable model accuracy (di Stefano et al., 2023), but it remains to be seen if the same level of rigour applied to the JUICE spacecraft will allow the long arcs to be fitted in a single estimation.

To prevent the misinterpretation of the results presented thus far, it must furthermore be emphasised that navigational tracking data can by no means act as a replacement for the radio science data. Considering the post-mission ephemeris generation, Fayolle et al. (2022) and Fayolle et al. (2024) have shown that a combination of 3GM and PRIDE VLBI (Gurvits et al., 2023) radio science data from the entire flyby tour yield more accurate moon ephemerides than what the navigation OD can achieve. The contribution of radio science data from the Ganymede orbit phase (Cappuccio et al., 2020) will improve the science ephemeris products even further. Furthermore, radio science data addresses other JUICE science goals, most notably the accurate determination of the moons gravity fields and tides (Cappuccio et al., 2020), which the navigation data cannot achieve.

Instead, this work suggests a possibly beneficial data synergy between the data from the navigation subsystem and radio science. Synergy between complementary observables from different data sources is expected to be a central aspect in the reconstruction of the JUICE trajectory and the generation of Galilean moon ephemerides (e.g. Morgado et al., 2019; Fayolle et al., 2024; Van Hoolst et al., 2024). Since scientific ephemeris generation will be most effective after the entire mission, it is not clear if the navigation data ability to enable a rapid improvement of the moon state knowledge during the flyby tour will be

of great advantage in this context. Inclusion of the navigation tracking measurements could nonetheless be beneficial. Even when considering the combined return from JUICE and Europa Clipper – both missions without flyby arcs or close approaches of Io – the radio science data set is unbalanced. With the dynamical signature of Io showing in the first arcs of the simulated navigation observations, the data from the navigation subsystem could help balance this data set. Similar considerations would likely apply to OpNav measurements of Io and Europa, and the data produced by the JANUS instrument (Della Corte et al., 2014) onboard the JUICE spacecraft, which were not investigated in this work.

It should be noted that synergising the radio science and navigation data sets, which are characterised by different accuracy and volume, requires careful weighting of the observations. This is very challenging, even more so when observations of entirely different data type (OpNav and JANUS) shall be included. Nevertheless, merging all available data in a single global inversion to estimate satellite ephemerides would allow the resulting ephemerides to reach the best possible level of accuracy. However, achieving this global inversion is contingent upon having a sufficiently consistent dynamical model for the spacecraft and the moons, as well as a well developed data treatment procedure. The addition of the navigation data, which will provide direct observations of the spacecraft state over longer time periods than the science data, will likely prove helpful in this process.

6. Conclusions

This work addresses potential synergies between the radiometric tracking data sets from the operational and scientific scope of the JUICE mission — specifically in relation to moon state knowledge for navigational operations and the generation of moon ephemerides for scientific purposes.

Using the Tudat software, the navigation orbit determination was simulated. The simulation results were successfully validated against the time evolution of the moon state uncertainty levels of the ESOC navigation setup (ESOC, 2017–2019).

We found that the navigation OD produces rapid and significant improvements of the moon state knowledge during the initial phase of the flyby tour, in particular for flyby moons. As a result, enhancing the navigation solution with ephemeris updates from radio-science was found to be of very limited influence. Cumulative savings by external moon ephemeris updates on the ΔV allocation for post-flyby clean-up manoeuvres were calculated to be $< 1\%$, corresponding to an estimated total saving of 0.78 m/s. This result was driven by the fact that the impact of ephemeris errors is a leading contributor only for the first series of flybys, where the navigation solution provides a much faster improvement of moon state knowledge than the ephemerides from science data which is collected only near the flybys themselves (Fayolle et al., 2022).

In order to effectuate more significant ΔV savings (up to 7.8% on clean-up allocation), it would be more advantageous to consider moon ephemeris improvements prior to the mission. These could be derived from ground-based astrometric measurements as well as data products from the Europa Clipper mission, which will arrive in the Jovian system before JUICE (Tarzi et al., 2019).

For a single flyby, the longer arc of observations on both sides of the moon encounter imposes tight constraints on the states of the system compared to the radio-science solution, despite the lower data quality. Furthermore, Io's direct dynamical signature on JUICE was detected in the observations collected priori to the 2G2 encounter, allowing its state to be constrained better. This indicates the potential for the navigation data to be used to improve post-mission system ephemerides. However, accurate modelling of the spacecraft dynamics, specifically of the non-conservative forces, along the long tracking arcs is challenging. It was shown that this is crucial for enabling a stable solution on arcs 2G2 and 3G3, and will determine the degree to which

---

[7] Here, it should be noted that if the *a priori* information on Io is reduced significantly compared to what is currently assumed, the navigation data on the first arcs may no longer provide any improvements. In addition, high-fidelity modelling of the dynamics of the JUICE spacecraft over the long arcs (which may otherwise not be required) could allow the number of empirical accelerations that are needed to be reduced, improving the stability of the solution. The degree to which this can be achieved may be limited by the manoeuvres performed by the spacecraft over these arcs.
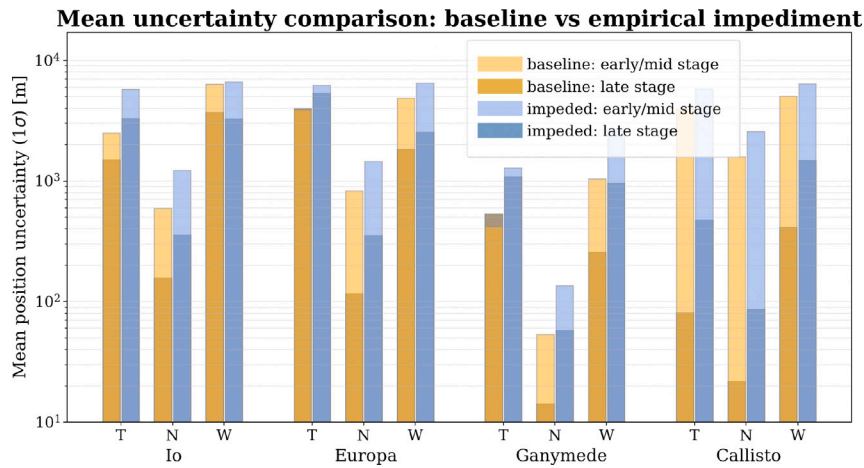
Fig. A.9. Average position uncertainty over early/mid and late mission stages, comparing post-arc uncertainty levels of the baseline and empirically impeded Navigation OD. Early/mid mission stage is defined up to (and including) arc 13C5.

the fast improvements in moon state knowledge can be realised during navigation operations.

The post-mission ephemerides that can be created using the data acquired by JUICE and Europa Clipper will be orders of magnitude more accurate than those currently available. Achieving the ultimate attainable quality will require significant work to be done in data fusion and dynamical modelling to maximise their quality (Magnanini et al., 2024; Fayolle et al., 2022, 2023b). The results in our work indicate the potential for the navigation data to contribute to this, either as part of the data used for the creation of the ephemerides, or as an independent data set used for validation and dynamical model refinement. The challenges involved in combining, and the exact role of, the various data types such as classical astrometry (Lainey et al., 2009), mutual events (Arlot and Emelyanov, 2019), mutual approximations (Fayolle et al., 2021), stellar occultations (Morgado et al., 2019), radar data (Brozović et al., 2020), space astrometry (Haw et al., 2000), VLBI from the PRIDE experiment (Fayolle et al., 2024), regular radio science data (Cappuccio et al., 2020) and navigation data (this manuscript) is currently under study. Achieving a consistent joint solution from these data will improve our knowledge of tidal parameters in the Jovian system, and help unravel the history of the orbits and interiors of the Galilean satellites.

CRediT authorship contribution statement

J. Hener: Writing – review & editing, Writing – original draft, Visualization, Validation, Software, Methodology, Formal analysis, Conceptualization. **S. Fayolle:** Writing – review & editing, Validation, Supervision, Software, Methodology, Conceptualization. **D. Dirkx:** Writing – review & editing, Validation, Supervision, Software, Methodology, Conceptualization.

Declaration of competing interest

The authors declare the following financial interests/personal relationships which may be considered as potential competing interests: Marie Fayolle reports financial support was provided by European Space Research and Technology Centre. Jonas Hener reports a relationship with European Space Research and Technology Centre that includes: employment.

Acknowledgements

Appendix. Empirical impediment of moon state evolution

In our implementation of the empirical impediment of moon state evolution we manipulate the covariance matrix such, that the formal errors of each moon are increased by a factor 5, i.e. the empirical factor ζ in Eq. (A.1) takes value 25. This factor is applied to the covariance matrix after the inversion on the given arc i and before the covariance is propagated to the following arc $i+1$ (Eq. (10)). This creates an increased *a priori* covariance on arc $i+1$, effectively deteriorating the moon state knowledge transfer between the arcs. In order to prevent the empirical deterioration to dominate the moon state knowledge evolution over the entire tour, we constrain the post-increase covariance of arc i to be no worse then the *a priori* covariance of the same arc.

In explicit terms, the empirically deteriorated moon covariance $\mathbf{P}^i_{\mathrm{m,prop}}$ to be propagated from arc i to arc $i+1$ is:

$$\left(\mathbf{P}^i_{\mathrm{m,prop}}\right)^{-1} = \left(\mathbf{P}^i_{\mathrm{m,0}}\right)^{-1} + \left(\zeta\,\mathbf{P}^i_{\mathrm{m}}\right)^{-1} \tag{A.1}$$

Naturally, the effect of this practice is a deteriorated moon state knowledge evolution over the course of the tour. Moon state knowledge improvement happens less rapidly and converges towards higher formal error levels at the end of the tour. The effect is quantitatively illustrated in Fig. A.9. Here it can be observed that the scheme serves its purpose: it deteriorates those state components most, which have been significantly improved by the baseline navigation filter (e.g. Ganymede *N* and *W*, Callisto *T* and *N*), while state components which are not improved greatly by the baseline filter do not deteriorate much.

In the navigation analysis performed for JUICE (ESOC, 2017–2019), no empirical deterioration of the moon state knowledge is implemented and has therefore not been included in our setup. If – for the sake of conservatism – during the JUICE GNC operations the moon state knowledge is degraded when transferred from one arc to the next, we expect that a similarly conservative approach would be applied to the moon state transferred from an external filter solution. Therefore we conclude that it is appropriate to conduct the comparative ΔV study on the base of the original, undegraded ephemeris solutions from both filters.

Data availability

Data will be made available on request.

References

Acton, Jr., C.H., 1996. Ancillary data services of nasa's navigation and ancillary information facility. Planet. Space Sci. 44 (1), 65–70.

Arlot, J.-E., Emelyanov, N., 2019. Natural satellites mutual phenomena observations: achievements and future. Planet. Space Sci. 169, 70–77.

Bellerose, J., Nandi, S., Roth, D., Tarzi, Z., Boone, D., Criddle, K., Ionasescu, R., 2016. Cassini navigation: The road to consistent subkilometer accuracy satellite encounters. In: AAS Annual Guidance and Control Conference.

Boone, D., Bellerose, J., Roth, D., 2017. Resolution of orbit determination prediction instabilities at Titan during Cassini's Solstice mission. In: International Symposium on Space Fight Dynamics.

Brozović, M., Nolan, M.C., Magri, C., Folkner, W.M., Jacobson, R.A., Harcke, L.J., McMichael, J.G., Richardson, J.E., Harmon, J.K., Taylor, P.A., et al., 2020. Arecibo radar astrometry of the galilean satellites from 1999 to 2016. Astron. J. 159 (4), 149.

Buffington, B., Strange, N., Ionasescu, R., 2005. Addition of a low altitude Tethys flyby to the nominal Cassini tour. In: AAS/AIAA Astrodynamics Specialist Conference.

Cappuccio, P., Di Benedetto, M., Durante, D., Iess, L., 2022. Callisto and europa gravity measurements from JUICE 3GM experiment simulation. Planetary Sci. J. 3 (8), 199.

Cappuccio, P., Hickey, A., Durante, D., Di Benedetto, M., Iess, L., De Marchi, F., Plainaki, C., Milillo, A., Mura, A., 2020. Ganymede's gravity, tides and rotational state from JUICE's 3GM experiment simulation. Planet. Space Sci. 187.

Cho, D.-H., Chung, Y., Bang, H., 2012. Trajectory correction maneuver design using an improved B-plane targeting method. Acta Astronaut. 72, 47–61.

D'Amario, L., Byrnes, D., Stanford, R., 1981. A new method for optimizing multiple-flyby trajectories. J. Guidance Control 4 (5), 591–596.

Della Corte, V., Schmitz, N., Zusi, M., Castro, J.M., Leese, M., Debei, S., Magrin, D., Michalik, H., Palumbo, P., Jaumann, R., et al., 2014. The JANUS camera onboard JUICE mission for Jupiter system optical imaging. In: Space Telescopes and Instrumentation 2014: Optical, Infrared, and Millimeter Wave. International Society for Optics and Photonics, p. 91433I.

di Stefano, I., Cappuccio, P., Iess, L., 2023. Precise modeling of non-gravitational accelerations of the spacecraft BepiColombo during cruise phase. J. Spacecr. Rockets 60 (5), 1625–1638.

Dirkx, D., Gurvits, L.I., Lainey, V., Lari, G., Milani, A., Cimò, G., Bocanegra-Bahamon, T., Visser, P., 2017. On the contribution of PRIDE-JUICE to jovian system ephemerides. Planet. Space Sci. 147, 14–27.

Dirkx, D., Lainey, V., Gurvits, L., Visser, P., 2016. Dynamical modelling of the Galilean moons for the JUICE mission. Planet. Space Sci. 134, 82–95.

Dirkx, D., Mooij, E., Root, B., 2019. Propagation and estimation of the dynamical behaviour of gravitationally interacting rigid bodies. Astrophys. Space Sci. 364 (2).

Dirkx, D., Prochazka, I., Bauer, S., Visser, P., Noomen, R., Gurvits, L.I., Vermeersen, B., 2018. Laser and radio tracking for planetary science missions — a comparison. J. Geod. 1–16.

Durante, D., Parisi, M., Serra, D., Zannoni, M., Notaro, V., Racioppa, P., Buccino, D., Lari, G., Gomez Casajus, L., Iess, L., et al., 2020. Jupiter's gravity field halfway through the juno mission. Geophys. Res. Lett. 47 (4), e2019GL086572.

ESA, 2014. JUICE Definition Study Report (Red Book). Technical Report.

ESOC, 2017–2019. JUICE: Navigation Analysis of the Jupiter Tour. Technical Report v1.1–v2.2, ESA.

Fayolle, M.S., Dirkx, D., Cimo, G., Gurvits, L.I., Lainey, V., Visser, P.N., 2024. Contribution of PRIDE VLBI products to the joint JUICE-Europa Clipper moons' ephemerides solution. Icarus 416, 116101.

Fayolle, M., Dirkx, D., Lainey, V., Gurvits, L., Visser, P., 2022. Decoupled and coupled moons' ephemerides estimation strategies application to the JUICE mission. Planet. Space Sci. 219, 105531.

Fayolle, M., Dirkx, D., Visser, P., Lainey, V., 2021. Analytical framework for mutual approximations-derivation and application to jovian satellites. Astron. Astrophys. 652, A93.

Fayolle, M., Lainey, V., Dirkx, D., Gurvits, L.I., Cimo, G., Bolton, S., 2023a. Spacecraft VLBI tracking to enhance stellar occultations astrometry of planetary satellites. Astron. Astrophys. 676, L6.

Fayolle, M., Magnanini, A., Lainey, V., Dirkx, D., Zannoni, M., Tortora, P., 2023b. Combining astrometry and JUICE-Europa Clipper radio science to improve the ephemerides of the galilean moons. Astronomy & Astrophysics 677, A42.

Folkner, W.M., Williams, J.G., Boggs, D.H., Park, R.S., Kuchynka, P., 2014. The planetary and lunar ephemerides DE430 and DE431. Interplanet. Netw. Progr. Rep. 196 (1), 42–196.

Fuller, J., Luan, J., Quataert, E., 2016. Resonance locking as the source of rapid tidal migration in the Jupiter and Saturn moon systems. Mon. Not. R. Astron. Soc. 458 (4), 3867–3879.

Grasset, O., Dougherty, M., Coustenis, A., Bunce, E., Erd, C., et al., 2013. Jupiter ICy moons explorer (JUICE): An ESA mission to orbit Ganymede and to characterise the Jupiter system. Planet. Space Sci. 78, 1–21.

Greenberg, R., 2010. The icy jovian satellites after the galileo mission. Rep. Progr. Phys. 73 (3), 036801.

Gurvits, L.I., Cimò, G., Dirkx, D., Pallichadath, V., Akins, A., Altobelli, N., Bocanegra-Bahamon, T.M., Cazaux, S.M., Charlot, P., Duev, D.A., et al., 2023. Planetary radio interferometry and Doppler experiment (PRIDE) of the JUICE mission. Space Sci. Rev. 219 (8), 79.

Haw, R., Antreasian, P., McElrath, T., Lewis, G., 2000. Galileo prime mission navigation. J. Spacecr. Rockets 37 (1), 56–63.

Hay, H.C., Trinh, A., Matsuyama, I., 2020. Powering the galilean satellites with moon-moon tides. Geophys. Res. Lett. 47 (15).

Hussmann, H., Spohn, T., 2004. Thermal-orbital evolution of Io and Europa. Icarus 171 (2), 391–410.

Ionasescu, R., Martin-Mur, T., Valerino, P., Criddle, K., Buffington, B., McElrath, T., 2014. Orbit determination covariance analysis for the Europa Clipper mission. In: AIAA Space 2014.

Lainey, V., Arlot, J.-E., Karatekin, Ö., Van Hoolst, T., 2009. Strong tidal dissipation in Io and Jupiter from astrometric observations. Nature 459 (7249), 957–959.

Lainey, V., Casajus, L.G., Fuller, J., Zannoni, M., Tortora, P., Cooper, N., Murray, C., Modenini, D., Park, R.S., Robert, V., et al., 2020. Resonance locking in giant planets indicated by the rapid orbital expansion of Titan. Nat. Astron. 4 (11), 1053–1058.

Lainey, V., Duriez, L., Vienne, A., 2004. New accurate ephemerides for the Galilean satellites of Jupiter - i. Numerical integration of elaborated equations of motion. Astron. Astrophys. 420 (3), 1171–1183.

Lainey, V., Tobie, G., 2005. New constraints on Io's and Jupiter's tidal dissipation. Icarus 179 (2), 485–489.

Lari, G., Milani, A., 2019. Chaotic orbit determination in the context of the JUICE mission. Planet. Space Sci. 176, 104679.

Lari, G., Saillenfest, M., Fenucci, M., 2020. Long-term evolution of the galilean satellites: the capture of callisto into resonance. Astron. Astrophys. 639, A40.

Magnanini, A., Zannoni, M., Casajus, L.G., Tortora, P., Lainey, V., Mazarico, E., Park, R.S., Iess, L., 2024. Joint analysis of JUICE and europa clipper tracking data to study the jovian system ephemerides and dissipative parameters. Astron. Astrophys. 687, A132.

Martin-Mur, T.J., Ionasescu, R., Valerino, P., Criddle, K., Roncoli, R., 2014. Navigational challenges for a Europa flyby mission. In: International Symposium on Space Flight Dynamics.

Montenbruck, O., Gill, E., 2000. Satellite Orbits: Models, Methods and Applications. Springer-Verlag Berlin Heidelberg.

Morgado, B., Benedetti-Rossi, G., Gomes-Júnior, A., Assafin, M., Lainey, V., Vieira-Martins, R., Camargo, J., Braga-Ribas, F., Boufleur, R., Fabrega, J., et al., 2019. First stellar occultation by the galilean moon europa and upcoming events between 2019 and 2021. Astron. Astrophys. 626.

Murrow, D., Jacobson, R., 1988. Galilean satellite ephemeris improvement using Galileo tour encounter information. In: Astrodynamics Conference. p. 4249.

Notaro, V., Durante, D., Iess, L., Bolton, S.J., 2021. Determination of jupiter's mass from juno radio tracking data. J. Guid. Control Dyn. 44 (5), 1062–1067.

Peale, S., 1999. Origin and evolution of the natural satellites. Annu. Rev. Astron. Astrophys. 37 (1), 533–602.

Raofi, B., Guman, M., Potts, C., 2000. Preliminary statistical analysis for a representative Europa orbiter mission. In: AIAA/AAS Astrodynamics Specialist Conference.

Schubert, G., Anderson, J., Spohn, T., McKinnon, W., 2004. Interior composition, structure and dynamics of the Galilean satellites. Jupiter: Planet, Satellites Magnetosph. 1, 281–306.

Tarzi, Z., Boone, D., Mastrodemos, N., Nandi, S., Young, B., 2019. Orbit determination sensitivity analysis for the Europa Clipper Mission tour. In: AIAA/AAS Space Flight Mechanics Meeting.

Van Hoolst, T., Tobie, G., Vallat, C., Altobelli, N., Bruzzone, L., Cao, H., Dirkx, D., Genova, A., Hussmann, H., Iess, L., et al., 2024. Geophysical characterization of the interiors of ganymede, callisto and europa by ESA's jupiter ICy moons explorer. Space Sci. Rev. 220 (5), 1–73.

Verma, A.K., Margot, J.-L., 2018. Expected precision of Europa Clipper gravity measurements. Icarus 314, 35–49.

Weeks, C., 2008. A statistical analysis of spacecraft maneuvers for a deep space mission. In: AIAA/AAS Astrodynamics Specialist Conference and Exhibit. p. 7194.

Wolf, A., Smith, J., 1995. Design of the cassini tour trajectory in the saturnian system. Control Eng. Pract. 3 (11), 1611–1619.